Iranian Journal of Numerical Analysis and Optimization
Vol. 16, No. 3, 2026, pp 757–788
https://doi.org/10.22067/ijnao.2026.97425.1826
https://ijnao.um.ac.ir/

Research Article

Analysis and optimal control of a proliferating-quiescent Glioma model with combined therapy

T. Jaber* and O. Balatif

Abstract

Low-grade gliomas (LGGs) are slow-growing but infiltrative brain tumors characterized by long-term persistence and frequent progression. In this work, we develop and analyze a compartmental mathematical model describing LGG dynamics under combination therapy involving cytotoxic chemotherapy and targeted molecular treatment. The tumor population is structured into proliferating, quiescent, and damaged compartments, and therapeutic interventions are incorporated through bilinear control terms accounting for chemo-therapies. We first establish the well-posedness of the model by proving existence, uniqueness, positivity, and boundedness of solutions. The dynamics of untreated glioma growth are then analyzed, revealing that the tumor-free equilibrium (TFE) is always unstable in the absence of therapy, leading to exponential tumor expansion. Under constant treatment regimens, we derive an explicit controlled reproduction number that governs tumor persistence or eradication. Using linearization and Lyapunov–LaSalle stability techniques, we establish necessary and sufficient conditions for both

*Corresponding author

Received 29 January 2026; revised 19 March 2026; accepted 17 April 2026

Tawfik Jaber
Laboratory of fundamental mathematics and their application, Department of Mathematics, Faculty of Sciences, Chouaib Doukkali University, El Jadida, Morocco. e-mail: jaber.tawfik@ucd.ac.ma

Omar Balatif
Laboratory of fundamental mathematics and their application, Department of Mathematics, Faculty of Sciences, Chouaib Doukkali University, El Jadida, Morocco. e-mail: balatif.maths@gmail.com

How to cite this article
Jaber, T. and Balatif, O., Analysis and optimal control of a proliferating-quiescent Glioma model with combined therapy. *Iran. J. Numer. Anal. Optim.*, 2026; 16(3): 757-788. https://doi.org/10.22067/ijnao.2026.97425.1826

local and global asymptotic stability of the tumor-free state. Finally, we formulate an optimal control problem to identify treatment strategies that minimize tumor burden while limiting therapeutic toxicity. The existence of optimal controls is rigorously proven using classical results from optimal control theory. Our results provide analytical insight into the stabilizing role of combination therapy and offer a quantitative guidance for designing optimized treatment protocols for LGG.

AMS subject classifications (2020): Primary 45D05; Secondary 42C10, 65G99.

Keywords: Bilinear models; Reproduction number; Glioma dynamics; Optimality conditions; Numerical simulations.

1 Introduction

Low-grade gliomas (LGGs) are a heterogeneous group of slow-growing primary brain tumors that originate from glial cells [15], typically classified as WHO grade II gliomas [27]. These tumors, although initially indolent, have the potential to undergo malignant transformation and progress to high-grade gliomas (e.g., glioblastoma) [41, 39]. LGGs commonly affect young adults, often presenting with seizures or neurological deficits and are associated with long-term morbidity [35]. Their infiltrative nature, resistance to complete surgical resection, and variable response to therapy make LGGs a challenging clinical and biological entity [5, 38]. Understanding their progression dynamics and developing effective, personalized treatment protocols are of crucial importance in neuro-oncology [39].

In the early years, treatment for LGGs mainly involved surgical resection, where doctors aimed to remove as much of the tumor as possible [18, 34]. After surgery, a watchful waiting approach was commonly used, especially in younger or lower-risk patients, because LGGs tend to grow slowly, and early surgical resection resulted in a clinically relevant survival benefit [20]. As more long-term data became available, it became clear that many LGGs eventually progress, and delaying treatment could reduce survival in high-risk patients. This led to the increased use of adjuvant treatments given after surgery, such as radiotherapy and chemotherapy. A major shift happened after the results of the RTOG 9802 clinical trial [37], which showed that combining radiotherapy with PCV chemotherapy (procarbazine, lomustine, and vincristine) significantly improved both progression-free survival and overall survival in patients with high-risk LGGs. In the 2000s and 2010s, temozolomide (TMZ) gained popularity as a chemotherapy option due to its oral administration, better tolerability, and promising clinical results [33]. It became the preferred chemotherapy for many patients, especially in cases where PCV was too toxic or

not tolerated. By the late 2010s and early 2020s, TMZ combined with radiotherapy became a common first-line treatment in clinical practice, especially for symptomatic or progressing tumors [29].

From a mathematical perspective, several models have been proposed to understand and simulate LGG growth and treatment response [17, 36]. Early models were primarily empirical, focusing on fitting exponential or logistic growth curves to tumor volume [4]. Later approaches incorporated compartmental models that distinguish between proliferative and quiescent tumor states [6]. Mathematical modeling has increasingly contributed to the understanding of LGG dynamics and treatment strategies. Several mathematical studies have been devoted to modeling the dynamics of LGGs and evaluating treatment strategies. In particular, the work in [8] investigates the nonlinear behavior of LGG growth through a system of differential equations, provides a detailed analysis of the system's stability in the absence of treatment, and demonstrates, through numerical simulations, how treatment timing and temozolomide dosing influence tumor progression. In [2], a mathematical model is constructed to investigate optimal combinations of chemotherapy and radiotherapy. Patient-specific parameters derived from imaging data inform in silico trials on a large virtual cohort, leading to the proposal of improved treatment schedules with potentially enhanced survival outcomes. The role of immunotherapy is explored in [21], where a coupled ordinary differential equation model captures the interactions between glioma cells, immune effectors, and adoptive cellular immunotherapy. Using Pontryagin's maximum principle, the authors formulate and solve an optimal control problem aimed at minimizing tumor burden and therapy-induced toxicity. Their analysis includes a characterization of the optimality system and demonstrates, through numerical solutions, the effectiveness of dynamically adjusted treatment strategies. Additionally, in [26], the authors examine the stability properties of a three-compartment model representing tumor cell-cycle dynamics under chemotherapy. They identify a critical drug dosage threshold above which global asymptotic stability of the TFE is guaranteed, and below which only local stability is achieved, with the existence of a bifurcation point separating treatment success from persistence.

However, many existing models fail to incorporate the bilinear structure of drug-tumor interaction, which is biologically relevant given that treatment efficacy often depends on both the drug concentration and tumor cell population [19, 3]. Additionally, few models combine the dynamics of multiple therapies (e.g., TMZ and IDH inhibitors) within a control-theoretic framework that respects pharmacokinetic constraints and clinical realities.

The remainder of the paper is organized as follows. In Section 2, we introduce the mathematical model describing the tumor tissue compartments and the therapeutic control mechanisms. Section 3 is devoted to the stability analysis of the uncontrolled system, including the characterization of the TFE. In Section 4, we investigate the local and global stability properties of the

controlled system under constant treatment strategies. Section 5 formulates the optimal control problem and derives the associated adjoint system together with the characterization of the optimal controls. Numerical simulations illustrating the theoretical results and highlighting the impact of optimal treatment strategies on tumor dynamics are presented in Section 6. Finally, Section 7 concludes the paper with a summary of the main findings and perspectives for future research.

2 Mathematical model of glioma dynamics

We present a compartmental mathematical model that describes the temporal evolution of LGG under the influence of combination therapy involving cytotoxic chemotherapy and targeted molecular therapy. The formulation is inspired by the chemotherapy-driven model introduced in [2], and is extended here to explicitly incorporate a second therapeutic modality through an additional bilinear control term, targeting isocitrate dehydrogenase (IDH) mutations, which are present in approximately 80% of LGG cases [16].

The tumor population is partitioned into three biologically distinct and mutually interacting compartments:

- $G_p(t)$: Proliferating tumor cells actively undergoing cell division.
- $G_q(t)$: Quiescent tumor cells in a reversible, nondividing state.
- $G_d(t)$: Damaged quiescent cells undergoing clearance or repair.

The dynamics of the system, illustrated by the flow diagram in Figure 1, are governed by the following system of ordinary differential equations:

$$\begin{aligned}
\frac{dG_p}{dt} &= \underbrace{\kappa G_p}_{\text{Proliferation}} - \underbrace{\tau_1 G_p}_{\text{Transition to quiescence}} + \underbrace{\tau_2 G_q}_{\text{Re-entry from quiescence}} \\
&\quad - \underbrace{\phi_1 u_1 G_p}_{\text{Chemo-induced damage}} - \underbrace{\phi_2 u_1 G_p}_{\text{Chemo-induced death}} - \underbrace{\kappa\omega u_2 G_p}_{\text{Targeted therapy inhibition}}, \\
\frac{dG_q}{dt} &= \underbrace{\tau_1 G_p}_{\text{Transition to quiescence}} - \underbrace{\tau_2 G_q}_{\text{Re-entry from proliferation}}, \\
\frac{dG_d}{dt} &= \underbrace{\phi_1 u_1 G_p}_{\text{Chemo-induced damage}} - \underbrace{\tau_3 G_d}_{\text{Clearance of damaged cells}},
\end{aligned} \tag{1}$$

where $u_1(t)$ and $u_2(t)$ represent time-dependent therapeutic controls bounded by $0 \leq u_i(t) \leq u_{i,\max} < 1$, with $i = 1, 2$.

2.1 Biological interpretation of model parameters

All state variables are assumed to be nonnegative and continuous for $t \geq 0$. The model parameters, all strictly positive, and have the following biological interpretations:

- **Proliferation rate ($\kappa > 0$)**: Represents the net growth rate of proliferating tumor cells, accounting for both birth and natural death processes. This parameter reflects the intrinsic aggressiveness of the glioma.
- **Transition rates ($\tau_1 > 0$, $\tau_2 > 0$)**:
  - τ_1: Rate at which proliferating cells enter quiescence, modeling reversible cell cycle arrest
  - τ_2: Rate at which quiescent cells re-enter proliferation, representing tumor plasticity
- **Therapeutic efficacy parameters**:
  - $\phi_1 > 0$: Rate of chemotherapy-induced DNA damage leading to damaged quiescent state
  - $\phi_2 > 0$: Rate of direct cytotoxic elimination of proliferating cells by chemotherapy
  - $\omega > 0$: Inhibition rate of proliferative capacity by IDH-targeted therapy
- **Clearance rate ($\tau_3 > 0$)**: Represents the rate at which damaged cells are removed from the system, either through apoptosis or immune-mediated clearance.

The total tumor burden is defined by $T(t) = G_p(t) + G_q(t) + G_d(t)$, and its evolution is implicitly regulated by the balance between proliferation, phenotypic transitions, therapeutic pressure, and damaged cell clearance, as described by system (1). Figure 1 provides a schematic representation of these interactions.

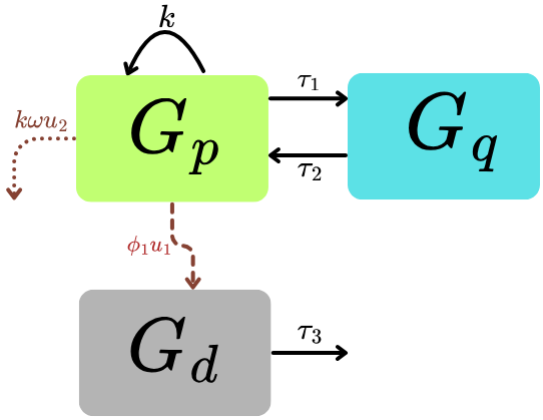

Figure 1: Flow diagram of the three-compartment tumor model. Compartments are colored, and arrows indicate transitions.

2.2 Mathematical well-posedness

From a mathematical perspective, the system (1) is well posed. Under standard assumptions on the continuity and local Lipschitz regularity of the right-hand side, the existence and uniqueness of solutions follow from classical results in the theory of ordinary differential equations [24]. Moreover, for any nonnegative initial condition, the solution remains nonnegative for all $t \geq 0$. This invariance property is essential for biological consistency and follows from the cooperative structure of the system and the absence of negative source terms acting on vanishing states [1, 10].

Theorem 1. For any initial condition $(G_p(0), G_q(0), G_d(0)) \in \mathbb{R}^3_+$ and measurable control functions $u_1, u_2 \in L^\infty([0,T])$ with $0 \leq u_i(t) \leq u_{i,\max}$, system (1) admits a unique absolutely continuous solution on $[0,T]$.

Proof. Let $\mathbf{x}(t) = (G_p(t), G_q(t), G_d(t))^\top$. The system (1) can be written as

$$\dot{\mathbf{x}}(t) = A(\mathbf{u}(t))\mathbf{x}(t),$$

where

$$A(\mathbf{u}) = \begin{bmatrix} \kappa(1-\omega u_2) - \tau_1 - (\phi_1+\phi_2)u_1 & \tau_2 & 0 \\ \tau_1 & -\tau_2 & 0 \\ \phi_1 u_1 & 0 & -\tau_3 \end{bmatrix}.$$

Define $f(t, \mathbf{x}, \mathbf{u}(t)) := A(\mathbf{u}(t))\mathbf{x}$. We verify the Carathéodory conditions for existence of solution to system (1)

(C1) Measurability in t: For each fixed $\mathbf{x}$, the map $t \mapsto f(t, \mathbf{x}, \mathbf{u}(t))$ is measurable because $\mathbf{u}(\cdot)$ is measurable and $A(\cdot)$ is continuous.

(C2) Continuity in $\mathbf{x}$: For each fixed t and $\mathbf{u}(t)$, the map $\mathbf{x} \mapsto f(t, \mathbf{x}, \mathbf{u}(t))$ is linear, hence continuous.

(C3) Lipschitz continuity in $\mathbf{x}$: Let $\|\cdot\|$ denote the Euclidean norm. For any $\mathbf{x}, \mathbf{y} \in \mathbb{R}^3$ and almost every $t \in [0, T]$, we have

$$\begin{aligned} \|f(t, \mathbf{x}, \mathbf{u}(t)) - f(t, \mathbf{y}, \mathbf{u}(t))\| &= \|A(\mathbf{u}(t))(\mathbf{x} - \mathbf{y})\| \\ &\leq \|A(\mathbf{u}(t))\| \cdot \|\mathbf{x} - \mathbf{y}\|, \end{aligned}$$

where $\|A\|$ denotes the induced matrix norm.
Let $M := \max\{|\kappa|, |\tau_1|, |\tau_2|, |\tau_3|, |\phi_1|, |\phi_2|, |\omega|\}$, and let $U_{\max} := \max\{u_{1,\max}, u_{2,\max}\}$. Using the Frobenius norm $\|A\|_F = \sqrt{\sum_{i,j} |a_{ij}|^2}$, we obtain the uniform bound

$$\|A(\mathbf{u}(t))\|_F \leq \sqrt{9M^2(1 + 4U_{\max}^2)} =: L.$$

Since all norms on $\mathbb{R}^{3\times 3}$ are equivalent, there exists $C > 0$ such that

$$\|A(\mathbf{u}(t))\| \leq C\|A(\mathbf{u}(t))\|_F \leq CL \quad \text{for a.e. } t \in [0, T].$$

Hence, f is Lipschitz continuous in $\mathbf{x}$ with constant CL.

(C4) Linear growth condition: For almost every $t \in [0, T]$, we have

$$\|f(t, \mathbf{x}, \mathbf{u}(t))\| \leq \|A(\mathbf{u}(t))\| \cdot \|\mathbf{x}\| \leq CL\|\mathbf{x}\|.$$

Since conditions (C1)–(C4) are satisfied, by the Carathéodory existence and uniqueness theorem for ordinary differential equations (see, e.g., [9]), there exists a unique absolutely continuous function $\mathbf{x} : [0, T] \to \mathbb{R}^3$ satisfying

$$\mathbf{x}(t) = \mathbf{x}_0 + \int_0^t f(s, \mathbf{x}(s), \mathbf{u}(s))\, ds \quad \text{for all } t \in [0, T].$$

□

Proposition 1. For nonnegative initial conditions, the solutions of (1) remain nonnegative for every $t \geq 0$.

Proof. We proceed by showing that the nonnegative orthant $\mathbb{R}^3_+$ is positively invariant. Consider the boundary faces of $\mathbb{R}^3_+$.

- If $G_p = 0$, then
$$\dot{G}_p = \tau_2 G_q \geq 0,$$
since $G_q \geq 0$ by the initial condition and continuity of solutions.
- If $G_q = 0$, then
$$\dot{G}_q = \tau_1 G_p \geq 0.$$
- If $G_d = 0$, then
$$\dot{G}_d = \phi_1 u_1 G_p \geq 0.$$

Equivalently, the system matrix $A(\mathbf{u}(t))$ is *quasi-positive* (Metzler) for all t, that is, all off-diagonal entries are nonnegative. Thus, by By Nagumo's invariance theorem [32], the set $\mathbb{R}^3_+$ is positively invariant. Consequently, for any nonnegative initial condition, the solution satisfies

$$\mathbf{x}(t) \in \mathbb{R}^3_+ \quad \text{for every } t \in [0, T].$$

□

Proposition 2. For bounded controls $0 \leq u_i(t) \leq u_{i,\max}$, the solutions of (1) remain bounded on any finite time interval $[0, T]$.

Proof. Let $M(t) = G_p(t) + G_q(t) + G_d(t)$. We get

$$\frac{dM}{dt} = \kappa(1 - \omega u_2)G_p - \phi_2 u_1 G_p - \tau_3 G_d \leq \kappa G_p \leq \kappa M.$$

By Gronwall's inequality, $M(t) \leq M(0)e^{\kappa t}$ for $t \in [0, T]$, establishing boundedness. □

3 Stability analysis of untreated glioma dynamics

Understanding the natural progression of glioma in the absence of therapeutic intervention is crucial for establishing baseline dynamics and quantifying the necessity of treatment. In this section, we conduct a stability analysis of the TFE for the uncontrolled system. This analysis serves two primary purposes: (1) to characterize the inherent growth dynamics of untreated glioma, and (2) to provide a reference point against which therapeutic efficacy can be evaluated.

Setting both therapeutic controls to zero ($u_1(t) = u_2(t) \equiv 0$) in the full model (1) yields the following autonomous system describing untreated glioma progression:

$$\begin{cases} \dfrac{dG_p}{dt} = \kappa G_p - \tau_1 G_p + \tau_2 G_q, \\ \dfrac{dG_q}{dt} = \tau_1 G_p - \tau_2 G_q, \\ \dfrac{dG_d}{dt} = -\tau_3 G_d. \end{cases} \tag{2}$$

Here all parameters are positive constants. We begin by identifying all steady-state solutions of (2).

Definition 1. A point $E^* = (G_p^*, G_q^*, G_d^*) \in \mathbb{R}^3_+$ is an equilibrium of system (2) if it satisfies

$$\left.\frac{dG_p}{dt}\right|_{E^*} = \left.\frac{dG_q}{dt}\right|_{E^*} = \left.\frac{dG_d}{dt}\right|_{E^*} = 0. \tag{3}$$

3.1 TFE

The TFE (tumor-free equilibrium), representing complete eradication of all tumor subpopulations, is given by

$$E_0 = (0, 0, 0). \tag{4}$$

This equilibrium exists unconditionally for all parameter values and represents the desired clinical outcome.

3.2 Existence of positive equilibria

To investigate the possibility of nontrivial steady states, we solve the system of algebraic equations obtained from (2):

$$0 = (\kappa - \tau_1) G_p^* + \tau_2 G_q^*, \tag{5}$$

$$0 = \tau_1 G_p^* - \tau_2 G_q^*, \tag{6}$$

$$0 = -\tau_3 G_d^*. \tag{7}$$

From (7), we immediately obtain $G_d^* = 0$, indicating that in the absence of therapy, no damaged cells persist at equilibrium. Equation (6) establishes a proportional relationship between quiescent and proliferating cells:

$$G_q^* = \frac{\tau_1}{\tau_2} G_p^*. \tag{8}$$

Substituting (8) into (5) yields

$$0 = (\kappa - \tau_1) G_p^* + \tau_2 \left(\frac{\tau_1}{\tau_2} G_p^* \right) = \kappa G_p^*. \tag{9}$$

Since $\kappa > 0$ by biological necessity (tumor cells possess positive proliferative capacity), (9) implies $G_p^* = 0$. Consequently, $G_q^* = 0$ from (8). This leads to the following important result.

Proposition 3. For the uncontrolled glioma system (2) with $\kappa > 0$, the TFE $E_0 = (0, 0, 0)$ is the only nonnegative equilibrium.

3.3 Local stability analysis of the TFE

We now investigate the local stability properties of E_0 using linearization techniques. The local stability determines whether infinitesimally small perturbations from the tumor-free state will decay (stable) or grow (unstable).

Theorem 2. The TFE E_0 of the uncontrolled system (2) is locally asymptotically unstable for all $\kappa > 0$. Specifically, E_0 is a saddle point with a one-dimensional unstable manifold and a two-dimensional stable manifold.

Proof. We linearize system (2) around E_0 by computing the Jacobian matrix:

$$J(E_0) = \begin{bmatrix} \frac{\partial f_1}{\partial G_p} & \frac{\partial f_1}{\partial G_q} & \frac{\partial f_1}{\partial G_d} \\ \frac{\partial f_2}{\partial G_p} & \frac{\partial f_2}{\partial G_q} & \frac{\partial f_2}{\partial G_d} \\ \frac{\partial f_3}{\partial G_p} & \frac{\partial f_3}{\partial G_q} & \frac{\partial f_3}{\partial G_d} \end{bmatrix}_{E_0} = \begin{bmatrix} \kappa - \tau_1 & \tau_2 & 0 \\ \tau_1 & -\tau_2 & 0 \\ 0 & 0 & -\tau_3 \end{bmatrix}, \tag{10}$$

where f_1, f_2, f_3 are the right-hand sides of equations in (2).

The eigenvalues of $J(E_0)$, denoted by $\lambda_1, \lambda_2, \lambda_3$, determine the local stability. Due to the block-triangular structure of $J(E_0)$, we can analyze the eigenvalues separately.

Eigenvalue from the damaged compartment:

The lower-right element gives $\lambda_1 = -\tau_3$. Since $\tau_3 > 0$, $\lambda_1 < 0$, indicating local stability in the G_d-direction.

Eigenvalues from the proliferating-quiescent subsystem:

The remaining eigenvalues come from the 2×2 submatrix:

$$J_{pq} = \begin{bmatrix} \kappa - \tau_1 & \tau_2 \\ \tau_1 & -\tau_2 \end{bmatrix}. \tag{11}$$

The characteristic polynomial of J_{pq} is

$$\begin{aligned} \det(J_{pq} - \lambda I_2) &= \det \begin{bmatrix} \kappa - \tau_1 - \lambda & \tau_2 \\ \tau_1 & -\tau_2 - \lambda \end{bmatrix} \\ &= (\kappa - \tau_1 - \lambda)(-\tau_2 - \lambda) - \tau_1\tau_2 \\ &= -\tau_2(\kappa - \tau_1 - \lambda) - \lambda(\kappa - \tau_1 - \lambda) - \tau_1\tau_2 \\ &= \lambda^2 + (\tau_1 + \tau_2 - \kappa)\lambda - \kappa\tau_2 = 0. \end{aligned} \tag{12}$$

Let λ_2 and λ_3 be the roots of (12). By Vieta's formulas,

$$\lambda_2 + \lambda_3 = -(\tau_1 + \tau_2 - \kappa) = \kappa - \tau_1 - \tau_2, \tag{13}$$

$$\lambda_2\lambda_3 = -\kappa\tau_2. \tag{14}$$

Since $\kappa > 0$ and $\tau_2 > 0$, (14) gives $\lambda_2\lambda_3 < 0$, which implies that λ_2 and λ_3 have opposite signs. Without loss of generality, assume $\lambda_2 < 0$ and $\lambda_3 > 0$.

To confirm the existence of a positive eigenvalue, we can evaluate the characteristic polynomial at $\lambda = 0$:

$$P(0) = -\kappa\tau_2 < 0.$$

Since $P(\lambda) \to +\infty$ as $\lambda \to +\infty$, by the Intermediate Value Theorem, there exists $\lambda_3 > 0$ such that $P(\lambda_3) = 0$.

Alternatively, applying Descartes' rule of signs to $P(\lambda) = \lambda^2 + (\tau_1 + \tau_2 - \kappa)\lambda - \kappa\tau_2$, the coefficient sequence is $[1, (\tau_1 + \tau_2 - \kappa), -\kappa\tau_2]$. There is exactly one sign change regardless of the sign of $(\tau_1 + \tau_2 - \kappa)$, guaranteeing exactly one positive real root.

all eigenvalues:

The complete set of eigenvalues is

$$\lambda_1 = -\tau_3 < 0, \tag{15}$$

$$\lambda_2 < 0, \tag{16}$$

$$\lambda_3 > 0. \tag{17}$$

Since there exists at least one eigenvalue with positive real part ($\lambda_3 > 0$), by Lyapunov's indirect method [22], the equilibrium E_0 is unstable. Moreover, with two negative eigenvalues and one positive eigenvalue, E_0 is classified as a saddle point. The stable manifold is two-dimensional (spanned by eigenvectors corresponding to λ_1 and λ_2), while the unstable manifold is one-dimensional (corresponding to λ_3).

This completes the proof of Theorem 2. □

3.4 Explicit growth rate and biological interpretation

The positive eigenvalue λ_3 can be computed explicitly from the quadratic formula applied to (12):

$$\lambda_3 = \frac{-(\tau_1 + \tau_2 - \kappa) + \sqrt{(\tau_1 + \tau_2 - \kappa)^2 + 4\kappa\tau_2}}{2}. \tag{18}$$

This expression represents the *net growth rate* of the glioma population in the absence of therapy.

Proposition 4. The growth rate λ_3 defined in (18) satisfies the following conditions:

1. $\lambda_3 > 0$ for all $\kappa > 0$, $\tau_1 > 0$, $\tau_2 > 0$.
2. λ_3 is increasing in κ: $\frac{\partial \lambda_3}{\partial \kappa} > 0$.
3. λ_3 satisfies $0 < \lambda_3 < \kappa$.

Proof. 1. The positivity follows from the analysis in Theorem 2.

2. Differentiating (18) with respect to κ, we have

$$\frac{\partial \lambda_3}{\partial \kappa} = \frac{1}{2}\left(1 + \frac{\tau_1 + \tau_2 - \kappa + 2\tau_2}{\sqrt{(\tau_1 + \tau_2 - \kappa)^2 + 4\kappa\tau_2}}\right) > 0.$$

3. From the characteristic polynomial $P(\lambda) = \lambda^2 + (\tau_1 + \tau_2 - \kappa)\lambda - \kappa\tau_2$, we have $P(\kappa) = \kappa^2 + (\tau_1 + \tau_2 - \kappa)\kappa - \kappa\tau_2 = \kappa\tau_1 > 0$. Since $P(0) = -\kappa\tau_2 < 0$ and $P(\kappa) > 0$, by the Intermediate Value Theorem, the positive root λ_3 satisfies $0 < \lambda_3 < \kappa$. □

3.5 Global dynamics and tumor progression

While local stability analysis characterizes behavior near equilibrium, we are also interested in the global behavior for biologically relevant initial conditions.

Proposition 5. The G_d equation in (2) is decoupled and can be solved analytically:

$$\frac{dG_d}{dt} = -\tau_3 G_d \quad \Rightarrow \quad G_d(t) = G_d(0)e^{-\tau_3 t}.$$

Thus, $G_d(t) \to 0$ exponentially for any initial condition $G_d(0) \geq 0$.

The dynamics of proliferating and quiescent cells are governed by the planar linear system:

$$\frac{d}{dt}\begin{bmatrix} G_p \\ G_q \end{bmatrix} = \begin{bmatrix} \kappa - \tau_1 & \tau_2 \\ \tau_1 & -\tau_2 \end{bmatrix}\begin{bmatrix} G_p \\ G_q \end{bmatrix}. \tag{19}$$

Theorem 3. For any initial condition $(G_p(0), G_q(0)) \neq (0, 0)$ with nonnegative components, the solution of (19) satisfies

$$\lim_{t\to\infty} \frac{1}{t} \log \|(G_p(t), G_q(t))\| = \lambda_3 > 0,$$

where λ_3 is given by (18). That is, the total tumor burden grows exponentially at rate λ_3.

Proof. System (19) is linear and homogeneous. Let $\mathbf{v}_2$ and $\mathbf{v}_3$ be eigenvectors corresponding to eigenvalues $\lambda_2 < 0$ and $\lambda_3 > 0$, respectively. The general solution is

$$\begin{bmatrix} G_p(t) \\ G_q(t) \end{bmatrix} = c_2 e^{\lambda_2 t}\mathbf{v}_2 + c_3 e^{\lambda_3 t}\mathbf{v}_3,$$

where c_2, c_3 are constants determined by initial conditions.

For generic initial conditions not aligned with the stable manifold (i.e., $c_3 \neq 0$), as $t \to \infty$,

$$\begin{bmatrix} G_p(t) \\ G_q(t) \end{bmatrix} \sim c_3 e^{\lambda_3 t}\mathbf{v}_3,$$

since $e^{\lambda_3 t}$ dominates $e^{\lambda_2 t}$ ($\lambda_3 > 0 > \lambda_2$). Therefore,

$$\|(G_p(t), G_q(t))\| \sim |c_3|\|\mathbf{v}_3\|e^{\lambda_3 t},$$

and

$$\lim_{t\to\infty} \frac{1}{t} \log \|(G_p(t), G_q(t))\| = \lambda_3 > 0.$$

□

Corollary 1. As $t \to \infty$, the ratio of quiescent to proliferating cells approaches

$$\lim_{t\to\infty} \frac{G_q(t)}{G_p(t)} = \frac{\tau_1}{\tau_2 + \lambda_3},$$

which is determined by the eigenvector $\mathbf{v}_3$ corresponding to λ_3.

4 Stability under constant therapy

We investigate the stability of the glioma dynamics under constant therapy inputs, where the control functions are fixed $u_1(t) = \tilde{u}_1 \in [0, u_{1,\max}]$ and $u_2(t) = \tilde{u}_2 \in [0, u_{2,\max}]$ reflecting a continuous and sustained treatment regime. The main objectives of this analysis are as follows: Establish conditions for tumor eradication by assessing the local stability of the TFE, characterize scenarios of treatment failure through the identification of endemic equilibria, and evaluate the stabilizing impact of IDH-targeted therapy on the proliferative tumor population. System (1) can reduced to a nonlinear autonomous system of ordinary differential equations:

$$\begin{aligned}
\frac{dG_p}{dt} &= (\kappa(1 - \omega\tilde{u}_2) - \tau_1 - (\phi_1 + \phi_2)\tilde{u}_1)G_p + \tau_2 G_q, \\
\frac{dG_q}{dt} &= \tau_1 G_p - \tau_2 G_q, \\
\frac{dG_d}{dt} &= \phi_1 \tilde{u}_1 G_p - \tau_3 G_d.
\end{aligned} \tag{20}$$

We analyze the system's equilibrium points and their local stability. The system admits a TFE at the origin $(G_p^*, G_q^*, G_d^*) = (0, 0, 0)$, which corresponds biologically to the eradication of all tumor subpopulations. In the case where $G_p^* \neq 0$, solving the steady-state conditions $\dot{G}_p = \dot{G}_q = \dot{G}_d = 0$ yields

$$\begin{aligned}
G_q^* &= \frac{\tau_1}{\tau_2} G_p^*, \\
G_d^* &= \frac{\phi_1 \tilde{u}_1}{\tau_3} G_p^*.
\end{aligned}$$

Substitution into the equation for G_p leads to the following critical condition for the existence of a nontrivial equilibrium:

$$\kappa(1-\omega\tilde{u}_2) = (\phi_1+\phi_2)\tilde{u}_1, \tag{21}$$

Remark 1. Equation (21) defines the threshold where therapeutic effects exactly balance tumor proliferation.

4.1 Local stability analysis

Theorem 4. The TFE point $(0,0,0)$ is locally asymptotically stable if and only if the controlled reproduction number [40, 11]

$$\mathcal{R}_0^{\text{controlled}} := \frac{\kappa(1-\omega\tilde{u}_2)}{(\phi_1+\phi_2)\tilde{u}_1},$$

satisfies $\mathcal{R}_0^{\text{controlled}} < 1$.

Proof. The Jacobian matrix J_0 of system (1) evaluated at the origin is therefore given by

$$J_0 = \begin{bmatrix} \kappa(1-\omega\tilde{u}_2) - \tau_1 - (\phi_1+\phi_2)\tilde{u}_1 & \tau_2 & 0 \\ \tau_1 & -\tau_2 & 0 \\ \phi_1\tilde{u}_1 & 0 & -\tau_3 \end{bmatrix}. \tag{22}$$

This Jacobian J_0 has an upper block-triangular structure, and the eigenvalues are thus composed of the following items:

1. $\lambda_1 = -\tau_3$, which is always negative, hence stable.

2. The remaining eigenvalues are obtained from the 2×2 upper-left submatrix:

$$J_2 = \begin{bmatrix} a & \tau_2 \\ \tau_1 & -\tau_2 \end{bmatrix}, \quad \text{where} \quad a = \kappa(1-\omega\tilde{u}_2) - \tau_1 - (\phi_1+\phi_2)\tilde{u}_1. \tag{23}$$

The characteristic polynomial for this submatrix is

$$\mathcal{X}_{J_2}(\lambda) = det(J_2 - \lambda.I_2) = \lambda^2 + (\tau_2 - a)\lambda - (a\tau_2 + \tau_1\tau_2) = 0. \tag{24}$$

Applying the Routh–Hurwitz criteria [12], local stability requires the following conditions:

- The trace condition: $\text{tr}(J_2) = a - \tau_2 < 0$,

- The determinant condition: $\det(J_2) = -a\tau_2 - \tau_1\tau_2 > 0$.

These two inequalities are simultaneously satisfied if and only if $a < -\tau_1$. This yields a critical threshold for the combined effect of the therapies. Defining the effective controlled reproduction rate $\mathcal{R}_0^{\text{controlled}}$ via

$$\mathcal{R}_0^{\text{controlled}} := \frac{\kappa(1-\omega\tilde{u}_2)}{(\phi_1+\phi_2)\tilde{u}_1}, \tag{25}$$

the condition $a < -\tau_1$ becomes equivalent to $\mathcal{R}_0^{\text{controlled}} < 1$. Thus, the TFE is locally asymptotically stable.

□

Remark 2. Although this threshold is derived directly from the Routh–Hurwitz criterion applied to the Jacobian of the linearized system, it exactly determines the local asymptotic stability of the TFE.

4.2 Global stability of the TFE

We now establish that, under a sufficient therapeutic regimen, the tumor-free state is the unique attractor for all biologically admissible initial conditions.

Theorem 5. If $\mathcal{R}_0^{\text{controlled}} < 1$, then the equilibrium $E_0 = (0,0,0)$ is globally asymptotically stable in the nonnegative orthant.

Proof. We work in $\mathbb{R}^3_+$ and introduce the linear Lyapunov function

$$V(G_p, G_q, G_d) \;=\; G_p \;+\; \frac{\tau_2}{\tau_1} G_q \;+\; \eta G_d,$$

where $\eta > 0$ will be chosen later. Clearly, $V > 0$ for any $(G_p, G_q, G_d) \neq (0,0,0)$, and $V = 0$ at E_0. Under constant controls $\tilde{u}_1, \tilde{u}_2$, the model reads

$$\begin{aligned}
\dot{G}_p &= a\, G_p + \tau_2\, G_q, \\
\dot{G}_q &= \tau_1\, G_p - \tau_2\, G_q, \\
\dot{G}_d &= \phi_1\, \tilde{u}_1\, G_p - \tau_3\, G_d,
\end{aligned}$$

where

$$a \;=\; \kappa(1-\omega\tilde{u}_2) - \tau_1 - (\phi_1+\phi_2)\,\tilde{u}_1.$$

Differentiating V along solutions gives

$$\begin{aligned}\dot{V} &= \dot{G}_p + \frac{\tau_2}{\tau_1}\dot{G}_q + \eta\dot{G}_d \\ &= aG_p + \tau_2 G_q + \frac{\tau_2}{\tau_1}(\tau_1 G_p - \tau_2 G_q) + \eta(\phi_1\tilde{u}_1 G_p - \tau_3\, G_d).\end{aligned}$$

We note by the construction that

$$\tau_2 G_p - \frac{\tau_2^2}{\tau_1} G_q = 0.$$

So transition terms cancel exactly, we obtain

$$\dot{V} = (a + \tau_2 + \eta\phi_1\tilde{u}_1)G_p - \eta\tau_3 G_d.$$

By taking $\eta = \frac{-(a+\tau_2)}{2\phi_1\tilde{u}_1} > 0$, small enough so that $a + \tau_2 + \eta\phi_1\tilde{u}_1 < 0$. Since $\kappa(1-\omega\tilde{u}_2) < (\phi_1+\phi_2)\,\tilde{u}_1$, which is exactly $\mathcal{R}_0^{\text{controlled}} < 1$. Under this hypothesis, $\dot{V}$ is strictly negative on $\mathbb{R}^3_+ \setminus \{E_0\}$. By LaSalle's invariance principle [25], all trajectories originating in $\mathbb{R}^3_+$ converge to the largest invariant subset of $\{\dot{V}=0\}$, namely the singleton $\{E_0\}$.

Hence, E_0 is globally asymptotically stable. □

Remark 3. The condition $a < -\tau_1$ (or equivalently, $\mathcal{R}_0^{\text{controlled}} < 1$ i.e. when the total therapeutic effect meets or exceeds the tumor proliferation rate) guarantees both local and global eradication of the tumor cell populations under constant therapy.

5 The optimal control problem

Among the chemotherapeutic agents commonly used in the treatment of LGGs, temozolomide remains a frontline therapy due to its ability to cross the blood-brain barrier and its cytotoxic activity against rapidly dividing tumor cells [31]. TMZ is an alkylating agent that introduces methyl groups into DNA, leading to DNA damage, replication stress, and apoptosis, particularly in proliferating tumor cells. In parallel, recent clinical advances have led to the approval of IDH inhibitors as targeted therapies for LGGs harboring IDH1 or IDH2 mutations [13]. IDH inhibitors act by suppressing the production of the oncometabolite 2-hydroxyglutarate, thereby reversing epigenetic dysregulation and promoting differentiation of tumor cells [30, 7]. Notably, IDH inhibitors exhibit a cytostatic effect that slows proliferation and may enhance the effectiveness of cytotoxic agents like TMZ when used in combination. In our model, we represent the cytotoxic control (TMZ) by the function $u_1(t)$, which governs the dose of chemotherapy administered over

time. A value of $u_1 = 0$ denotes no drug use, while $u_1 = u_{1,\max}$ corresponds to the maximum tolerable dose, constrained within the range $0 \leq u_1(t) \leq u_{1,\max} < 1$. The targeted IDH inhibitor is modeled by the control $u_2(t)$, with $u_2 = 0$ indicating absence of the therapy and $u_2 = u_{2,\max}$ corresponding to full inhibition. The dosage range is similarly bounded as $0 \leq u_2(t) \leq u_{2,\max} < 1$. Both therapies are assumed to act bilinearly on the proliferating tumor compartment, with TMZ reducing the growth and survival of dividing cells and the IDH inhibitor modulating the tumor microenvironment and the metabolic state of resistant or quiescent cells. By integrating these two mechanisms into our bilinear model, we aim to capture the synergistic dynamics of dual-agent treatment and better inform optimized therapy schedules for LGG patients. Unlike prior studies that evaluate system behavior under fixed or time-invariant treatment intensities, our analysis investigates the tumor dynamics under time-dependent optimal control strategies. Specifically, we consider therapeutic inputs $u_1(t)$ and $u_2(t)$ as measurable functions of time, optimized to minimize tumor burden and treatment cost over a fixed treatment horizon $[0, T]$.

The objective function to be minimized is defined as

$$J(u_1, u_2) = \int_0^T \left(A_1 G_p(t) + A_2 G_q(t) + \tfrac{1}{2} B_1 u_1^2(t) + \tfrac{1}{2} B_2 u_2^2(t) \right) dt, \tag{26}$$

where $G_p(t)$ and $G_q(t)$ represent, respectively, the proliferating and quiescent tumor cell populations at time t, and $A_i > 0$ and $B_i > 0$ $(i = 1, 2)$ are fixed weighting coefficients that reflect the relative importance of reducing tumor burden and minimizing the therapeutic dosing effort.

We seek optimal control functions $u_1^*(t)$ and $u_2^*(t)$ that minimize the cost functional J, that is,

$$J(u_1^*, u_2^*) = \min_{(u_1, u_2) \in \mathcal{U}_{ad}} J(u_1, u_2), \tag{27}$$

where the set of admissible controls $\mathcal{U}_{ad}$ is defined as follows:

$$\mathcal{U}_{ad} = \{(u_1(t), u_2(t)) \in L^\infty(0, T)^2; \quad 0 \leq u_i(t) \leq u_{i,\max} < 1, \text{ for } i = 1, 2\}. \tag{28}$$

This optimal control framework allows us to identify therapy protocols that minimize the tumor size and overall tumor burden throughout the treatment period, while penalizing high doses of TMZ and the IDH inhibitor to reduce toxicity and cost.

5.1 Existence of optimal control solutions

We establish the existence of an optimal control pair $(u_1^*, u_2^*) \in \mathcal{U}_{ad}$ for the control problem governed by the bilinear system (1) and the cost functional (26), using a standard result from optimal control theory (see [14, Corollary 4.1]).

Theorem 6. Consider the optimal control problem defined by system (1) with the objective functional (26). There exists an optimal control pair $(u_1^*, u_2^*) \in \mathcal{U}_{ad}$ such that

$$J(u_1^*, u_2^*) = \min_{(u_1,u_2)\in\mathcal{U}_{ad}} J(u_1, u_2).$$

Proof. To guarantee existence of optimal controls, we verify the following standard conditions:

1. **Nonemptiness of admissible controls and corresponding state trajectories:** Let the state vector be $x = (G_p, G_q, G_d)$ with the right-hand side of the system (1) given by $\dot{x} = F(t, x, u_1, u_2)$. Since the system is bilinear in u_1 and u_2, and all coefficients and parameters are continuous and bounded, and the controls are bounded measurable functions, the right-hand side is Lipschitz continuous in x. Therefore, by the Picard–Lindelof theorem, for any admissible control $(u_1, u_2) \in \mathcal{U}_{ad}$, there exists a unique solution $x(t) \in C^1([0, T]; \mathbb{R}^3)$ satisfying the initial conditions. Hence, the set of admissible control-state pairs is nonempty.

2. **Convexity and closedness of the control set:** From the definition of the controls set (28), it is clear that $\mathcal{U}_{ad}$ is a product of closed intervals in L^∞, hence convex and closed.

3. **Bilinearity of the system in control variables:**
The state system (1) is bilinear in u_1 and u_2 with coefficients depending continuously on the state and time. Since the state trajectories are bounded (due to biologically relevant constraints and bounded control functions), the function $F(t, x, u_1, u_2)$ is continuous and satisfies the required regularity conditions.

4. **Convexity and lower boundedness of the integrand in the cost functional:**
The cost functional is of the form:

$$J(u_1, u_2) = \int_0^T \left(\sum_{i=1}^{2} A_i x_i(t) + \frac{1}{2} B_1 u_1(t)^2 + \frac{1}{2} B_2 u_2(t)^2 \right) dt.$$

This integrand is convex in the controls u_1, u_2, because it is a positive definite quadratic form in u_1 and u_2. Moreover, since $L(t, x, u_1, u_2) \geq (B1/2)u_1^2 + (B_2/2)u_2^2 \geq c_2(|u_1^2| + |u_2^2|)$

with $c_2 = \min(B_1/2, B_2/2)$, $\xi = 2$, and $L \geq 0$, together with the uniform boundedness of trajectories on $[0, T]$(Proposition 2), the standard coercivity and compactness conditions of optimal control theory are satisfied (e.g., [14]).

All hypotheses of the Fleming–Rishel existence theorem are verified. Therefore, there exists an optimal control pair $(u_1^*, u_2^*) \in \mathcal{U}_{ad}$ minimizing the objective functional $J(u_1, u_2)$. □

5.2 Characterization of an optimal controls

To derive the necessary conditions for optimality in the LGG therapy model, we employ Pontryagin's maximum principle [23]. This principle introduces a set of adjoint variables that link the state dynamics with the cost functional through a Hamiltonian function. The optimization problem is thus reformulated as a two-point boundary value problem: The state variables evolve forward in time with known initial conditions, while the adjoint variables evolve backward from known terminal conditions. The optimality system consists of the state equations, adjoint equations, and pointwise minimization of the Hamiltonian with respect to the control variables, subject to their admissible bounds. This structured approach provides a powerful framework to characterize the optimal therapeutic strategy.

The Hamiltonian associated with the problem is defined as

$$\mathcal{H}(t) = A_1 G_p(t) + A_2 G_q(t) + \frac{1}{2} B_1 u_1^2(t) + \frac{1}{2} B_2 u_2^2(t) + \lambda_1 f_1 + \lambda_2 f_2 + \lambda_3 f_3, \tag{29}$$

where the functions f_i for $i = 1, 2, 3$ represent the right-hand sides of the system of differential equations (1), and λ_i are the adjoint functions. Therefore

$$\begin{aligned}
f_1(G_p, G_q, G_d, u_1, u_2) &= \kappa(1 - \omega u_2) G_p - \tau_1 G_p + \tau_2 G_q - \phi_1 u_1 G_p - \phi_2 u_1 G_p, \\
f_2(G_p, G_q, G_d, u_1, u_2) &= \tau_1 G_p - \tau_2 G_q, \\
f_3(G_p, G_q, G_d, u_1, u_2) &= \phi_1 u_1 G_p - \tau_3 G_d.
\end{aligned}$$

Theorem 7. Let $(u_1^*, u_2^*) \in \mathcal{U}_{ad}$ be an optimal control pair minimizing the cost functional $J(u_1, u_2)$, subject to the system dynamics (1) and the admissible control set $\mathcal{U}_{ad}$. Then, there exist adjoint functions $\lambda_1(t), \lambda_2(t), \lambda_3(t)$ satisfying the adjoint system

$$\begin{cases} \dot{\lambda}_1 = -A_1 - \lambda_1(\kappa(1-\omega u_2) - \tau_1 - (\phi_1+\phi_2)u_1) - \lambda_2\tau_1 - \lambda_3\phi_1 u_1, \\ \dot{\lambda}_2 = -A_2 - \lambda_1\tau_2 + \lambda_2\tau_2, \\ \dot{\lambda}_3 = \lambda_3\tau_3, \end{cases} \tag{30}$$

with terminal conditions

$$\lambda_1(T) = \lambda_2(T) = 0.$$

Furthermore, the optimal controls $u_1^*(t), u_2^*(t)$ are characterized by

$$\begin{aligned} u_1^*(t) &= \min\left(1, \max\left(0, \frac{((\phi_1+\phi_2)\lambda_1(t) - \phi_1\lambda_3(t))G_p(t)}{B_1}\right)\right), \\ u_2^*(t) &= \min\left(1, \max\left(0, \frac{\kappa\omega\lambda_1(t)G_p(t)}{B_2}\right)\right). \end{aligned} \tag{31}$$

Proof. For $t \in [0,T]$, the adjoint equations and the transversality conditions can be derived using the the Pontryagin's maximum principle [23], such that

$$\begin{aligned} \dot{\lambda}_1 &= -\frac{\partial \mathcal{H}}{\partial G_p} = -A_1 - \lambda_1(\kappa(1-\omega u_2) - \tau_1 - (\phi_1+\phi_2)u_1) - \lambda_2\tau_1 - \lambda_3\phi_1 u_1, \\ \dot{\lambda}_2 &= -\frac{\partial \mathcal{H}}{\partial G_q} = -A_2 - \lambda_1\tau_2 + \lambda_2\tau_2, \\ \dot{\lambda}_3 &= -\frac{\partial \mathcal{H}}{\partial G_d} = \lambda_3\tau_3, \end{aligned} \tag{32}$$

The Hamiltonian minimization condition requires that, at the optimal solution, derive $\mathcal{H}$ with respect to the controls and setting the derivatives to zero gives the following system:

$$\begin{aligned} \frac{\partial \mathcal{H}}{\partial u_1} &= B_1 u_1 - \lambda_1(\phi_1+\phi_2)G_p + \lambda_3\phi_1 G_p = 0, \\ \frac{\partial \mathcal{H}}{\partial u_2} &= B_2 u_2 - \lambda_1\kappa\omega G_p = 0. \end{aligned} \tag{33}$$

It follows

$$\begin{aligned} u_1 &= \frac{((\phi_1+\phi_2)\lambda_1 - \phi_1\lambda_3)G_p}{B_1}, \\ u_2 &= \frac{\kappa\omega\lambda_1 G_p}{B_2}. \end{aligned}$$

Applying the control constraints, we project each expression onto the admissible interval:

$$\begin{aligned} u_1^*(t) &= \min\left(1, \max\left(0, \frac{((\phi_1+\phi_2)\lambda_1 - \phi_1\lambda_3)G_p}{B_1}\right)\right), \\ u_2^*(t) &= \min\left(1, \max\left(0, \frac{\kappa\omega\lambda_1 G_p}{B_2}\right)\right). \end{aligned}$$

□

6 Numerical simulations

To assess the performance of the proposed optimal control strategy, we carried out numerical simulations using the forward-backward sweep method (FBSM), a well-established iterative algorithm for solving optimal control problems governed by systems of ordinary differential equations [28]. The method alternates between forward integration of the state equations and backward integration of the adjoint equations, followed by an update of the control variables based on the optimality conditions derived from Pontryagin's maximum principle. This iterative process is repeated until convergence, defined in terms of the normed difference between successive control iterates falling below a prescribed tolerance.

The state system was solved forward in time using a fourth-order Runge–Kutta scheme, while the adjoint system was integrated backward in time under the terminal conditions $\lambda_i(T) = 0$. At each iteration, the optimal controls were updated via projection onto the admissible control set, ensuring biologically feasible treatment intensities. Convergence was typically achieved within a small number of iterations, indicating numerical stability and robustness of the proposed algorithm.

Model parameters were calibrated using clinical data reported in [36], which provide longitudinal measurements of LGG size in patients treated with temozolomide. Tumor burden was quantified through the mean tumor diameter (in millimeters), consistent with clinical practice. When necessary, tumor volumes were reconstructed assuming spherical geometry. The model was formulated in normalized (dimensionless) form by scaling tumor cell densities with respect to a reference carrying capacity K, representing the maximal viable tumor cell density in brain tissue. Consequently, the state variables $0 \leq P, Q, D \leq 1$. Initial conditions were inferred from early diagnostic imaging and chosen to reflect biologically realistic compartment proportions observed in LGG. Specifically, the initial proliferative fraction was set to $P(0) = 0.01$, and the quiescent fraction to $Q(0) = 0.09$, yielding an initial total tumor burden corresponding to 10% of the carrying capacity. No damaged cells were assumed at treatment initiation, so $D(0) = 0$.

This choice reflects the known predominance of quiescent cells in LGGs, together with a smaller actively proliferating subpopulation prior to therapy.

The simulation horizon was fixed at 25 months in order to capture both short-term treatment effects and long-term tumor dynamics. The parameter values reported in Table 1 are used for illustrative purposes; the qualitative behavior of the system depends primarily on the structural

interactions among proliferation, quiescence, and treatment effects rather than on the precise numerical values.

Table 1: The parameters κ, τ_1, τ_2, τ_3, ϕ_1, ϕ_2 are taken from the clinical tumor growth inhibition model developed by Ribba et al. in their LGG TMZ-only work [36]. These parameters were originally estimated by fitting longitudinal MRI tumor size data under temozolomide therapy. All rates are expressed in month^{-1}.

Parameter	**Description**	**Value**
κ	Natural proliferation rate of tumor cells	0.114
τ_1	Transition rate from proliferative to quiescent state	0.0226
τ_2	Transition rate from quiescent to proliferative state	0.0045
τ_3	Clearance rate of damaged tumor cells	0.0214
ϕ_1	TMZ-induced damage rate on proliferative cells	0.842
ϕ_2	Cytotoxic effect of TMZ on proliferative cells	0.32
ω	Effect rate of IDH inhibitor on proliferative cells	0.3

The IDH-inhibitor efficacy $\omega = 0.2$ month^{-1} is chosen as a conservative estimate of cytostatic slowdown based on emerging IDH-inhibitor data (e.g., reduced proliferation without strong cytotoxicity). Sensitivity to ω is explored in simulations. Here, we investigate two distinct control strategies over a 30-month treatment horizon:

- **Strategy 1:** IDH-inhibitor monotherapy (cytostatic control $u_2(t)$ only, $u_1(t) \equiv 0$),
- **Strategy 2:** Combined therapy with temozolomide (cytotoxic control $u_1(t)$) and IDH-inhibitor (cytostatic control $u_2(t)$).

The objective is to compare the qualitative and quantitative tumor responses under purely proliferation-slowing treatment versus dual cytotoxic–cytostatic intervention.

Uncontrolled dynamics

In the absence of treatment, the proliferating tumor cell population (G_p) grows exponentially (Figure 2), reflecting the intrinsic instability of the untreated system. This behavior reproduces the characteristic slow but persistent progression of LGG. Simultaneously, the quiescent compartment (G_q) gradually accumulates (Figure 3) , forming a latent reservoir capable of sustaining future tumor regrowth. As expected, the damaged compartment (G_d) remains identically zero without therapy (Figure 4).

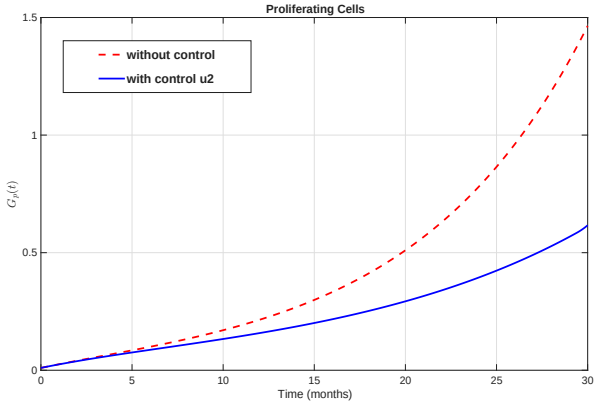

Figure 2: Dynamics of proliferating compartment (G_p) with control u_2 only.

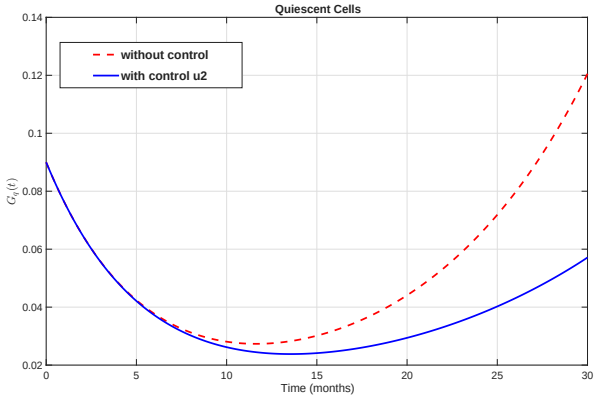

Figure 3: Dynamics of quiescent compartment (G_q) with control u_2 only.

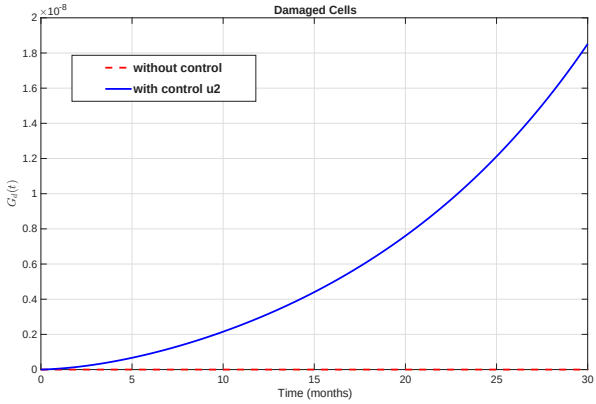

Figure 4: Dynamics of damaged compartment (G_d) with control u_2 only.

Strategy 1: IDH-inhibitor monotherapy (cytostatic control)

In this part of the simulations, we consider the optimal cytostatic control $u_2(t)$ alone, with $u_1(t) \equiv 0$. As shown in Figure 2, the proliferating cell population G_p exhibits a marked reduction compared to the uncontrolled case. The IDH-inhibitor acts by decreasing the effective proliferation rate, thereby slowing tumor expansion rather than inducing direct cell death. Consequently, G_p does not undergo complete eradication but instead converges toward a lower stabilized level, reflecting tumor growth containment rather than elimination. Quantitatively, the proliferating population decreases from a peak value exceeding 1.5 units to approximately 0.6 units after treatment, demonstrating substantial but partial suppression of tumor activity.

As shown in Figure 3, the quiescent compartment G_q decreases indirectly under IDH-inhibitor monotherapy, dropping from approximately 0.12 to less than 0.06. This reduction results from the cytostatic action of $u_2(t)$, which lowers the effective proliferation rate and consequently limits the flux of newly generated cells transitioning into the quiescent state. Importantly, because the IDH inhibitor is modeled as a purely cytostatic agent, the damaged compartment G_d remains negligible during therapy.

Strategy 2: Combined TMZ and IDH Therapy

When both controls are active, a markedly stronger therapeutic effect is observed. The proliferating compartment G_p rapidly declines toward near-zero levels (Figure 5), demonstrating the synergistic effect of cytotoxic killing $u_1(t)$ and proliferation slowdown $u_2(t)$. This combined action not only halts tumor growth but actively reduces tumor burden.

The quiescent population G_q also progressively decreases to near zero, as shown in (Figure 6). Although its decline is slower than that of G_p, the sustained reduction reflects both diminished inflow from proliferating cells and indirect effects of cytotoxic depletion. The gradual elimination of this dormant reservoir is critical to minimizing recurrence risk.

In contrast to monotherapy, the damaged compartment G_d (Figure 7) emerges exclusively under TMZ administration. Its monotonic increase during treatment serves as a marker of irreversible tumor cell inactivation. The accumulation of G_d, together with its clearance dynamics, illustrates the long-term reduction in the tumor's effective reproductive capacity achieved through cytotoxic intervention.

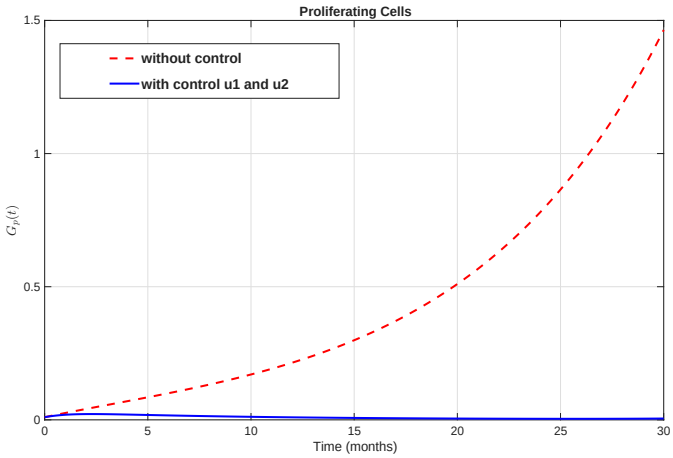

Figure 5: Dynamics of proliferating compartment (G_p) with controls u_1 and u_2.

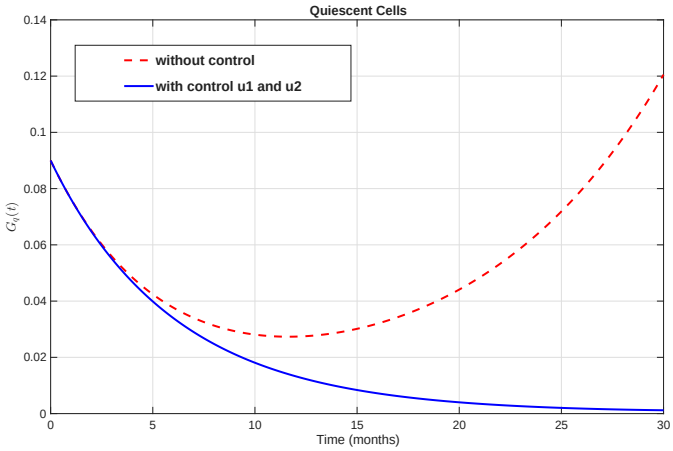

Figure 6: Dynamics of quiescent compartment (G_q) with controls u_1 and u_2.

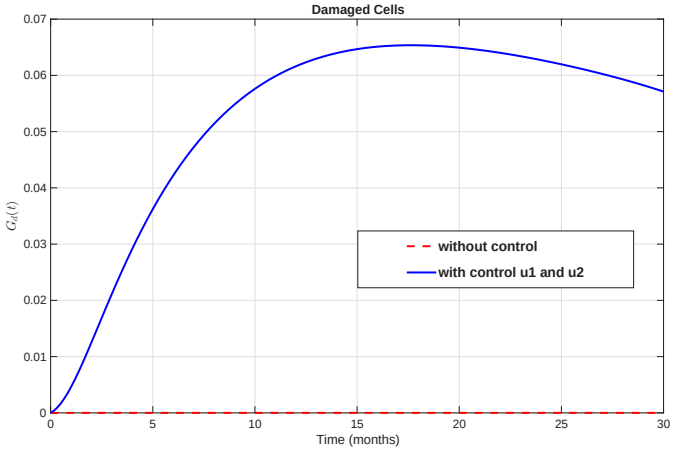

Figure 7: Dynamics of damaged compartment (G_d) with controls u_1 and u_2.

Remark 4. The simulations highlight a fundamental difference between the two strategies. IDH-inhibitor monotherapy achieves tumor growth stabilization through cytostatic slowing of proliferation but does not induce substantial irreversible tumor reduction. In contrast, the combined TMZ–IDH therapy simultaneously suppresses active proliferation, depletes the quiescent reservoir, and generates irreversible cellular damage, leading to sustained tumor control.

From a clinical perspective, these results suggest that cytostatic maintenance alone may contain tumor progression, whereas combination therapy is required to achieve significant tumor burden reduction and long-term disease stabilization.

7 Conclusion

In this study, we developed a bilinear compartmental model to describe LGG dynamics under combined therapy with temozolomide (TMZ) chemotherapy and IDH-targeted treatment. The model includes important biological processes such as the reversible transition between proliferating and quiescent tumor cells, therapy-induced damage, and removal of damaged cells.

Mathematically, we showed that the system is well-posed: Solutions exist, are unique, remain positive, and are bounded for any admissible control. The analysis of the system without treatment showed that the TFE is unstable, meaning the tumor will grow if left untreated. This highlights the need for therapy to control tumor growth.

For constant treatments, we defined a threshold parameter, called the controlled reproduction number, which measures the balance between tumor growth and therapy. When this number is below one, the TFE becomes stable, showing that constant therapy at sufficient intensity can stop tumor growth. This demonstrates the benefit of combining TMZ and IDH-targeted therapy.

We also solved an optimal control problem to find the best time-dependent treatment schedules that reduce tumor size while keeping drug use reasonable. The numerical results show that the optimal controls start with a strong initial dose, then remain nearly constant for a long period, and finally decrease gradually. This pattern matches the theoretical stability results: Once the tumor is under control, maintaining it with a steady treatment is enough. The long constant phase suggests that a maintenance-like strategy can be effective while limiting side effects.

Overall, this study shows that combining mathematical modeling, stability analysis, and optimal control can help design effective treatment strategies for LGG. The results could be useful for developing personalized treatment plans that balance tumor control with patient well-being.

Funding

This research received no external funding.

Conflicts of Interest

All authors jointly worked on the results and they read and approved the final manuscript, and also declare that they have no competing interests.

References

[1] Andrica, D., and Rassias, T. *Differential and integral inequalities*, Cham: Springer, 2019.

[2] Ayala-Hernández, L.E., Gallegos, A., Schucht, P., Murek, M., Pérez-Romasanta, L., Belmonte-Beitia, J. and Pérez-García, V.M. *Optimal combinations of chemotherapy and radiotherapy in low-grade gliomas: a mathematical approach*, J. Pers. Med., 11(10) (2021), 1036.

[3] Balatif, O., and Rachik, M., and Rachik, Z. *Optimal control for multi-input bilinear systems with an application in cancer chemotherapy*, Int. J. Sci. Innov. Math. Res. (IJSIMR), 3 (2015), 22–31.

[4] Benzekry, S., Lamont, C., Beheshti, A., Tracz, A., Ebos, J.M., Hlatky, L. and Hahnfeldt, P. *Classical mathematical models for description and prediction of experimental tumor growth*, PLoS Comput. Biol., 10(8) (2014), e1003800.

[5] Bodnar, M., Vela-Pérez, M. and Tryniecka-Maciek, A. *Analyzing the impact of proliferation and treatment parameters on low-grade glioma growth using mathematical models*, Physica D, 472 (2025), 134491.

[6] Bull, J.A., Mech, F., Quaiser, T., Waters, S.L. and Byrne, H.M. *Mathematical modelling reveals cellular dynamics within tumour spheroids*, PLoS Comput. Biol., 16(8) (2020), e1007961.

[7] Cai, Z., Yang, H., Yu, Z., Su, J., Zhang, J., Ye, Z., Hu, K., Huang, T. and Zhou, H. *Efficacy and safety of IDH inhibitors in IDH-mutated cancers: a systematic review and meta-analysis of 4 randomized controlled trials*, World J. Surg. Oncol., 22(1) (2024), 295.

[8] Carmona-Moreno, F.J., Gallegos, A., Barba-Franco, J.J., Urenda-Cázares, E., Jiménez-Guerrero, E.V. and Macías-Díaz, J.E. *Dynamics analysis of nonlinear differential equation systems applied to low-grade gliomas and their treatment*, Foundations, 5(1) (2025), 6.

[9] Coddington, E.A., and Levinson, N. *Theory of ordinary differential equations*, New York: McGraw-Hill, 1955.

[10] Davarian, N., Heydari, A., Hashemi Mehne, S.H. and Heydari, A.A. *The investigation of stability and optimal control of the multigroup Covid-19 epidemic model in Iran*, J. Math. Exten., 19(1) (2025), 1–32.

[11] Diekmann, O., Heesterbeek, J.A.P., and Metz, J.A.J. *On the definition and the computation of the basic reproduction ratio R0 in models for infectious diseases in heterogeneous populations*, J. Math. Biol., 28(4) (1990), 365–382.

[12] Edelstein-Keshet, L. *Mathematical models in biology*, Philadelphia: SIAM, 2005.

[13] Eisenstein, M. *FDA approves first IDH-targeted glioma drug*, Nature Portfolio News, 2024.

[14] Fleming, W.H., and Rishel, R.W. *Deterministic and stochastic optimal control*, New York: Springer, 2012.

[15] Forst, D.A., Nahed, B.V., Loeffler, J.S. and Batchelor, T.T., *Low-grade gliomas*, Oncologist, 19(4) (2014), 403–413.

[16] Han, S., Liu, Y., Cai, S.J., Qian, M., Ding, J., Larion, M., Gilbert, M.R. and Yang, C. *IDH mutation in glioma: molecular mechanisms and potential therapeutic targets*, Br. J. Cancer, 122(11) (2020), 1580–1589.

[17] Handoko, H., Wahyudi, S.T., Setyawan, A.A. and Kartono, A. *A dynamical model of combination therapy applied to glioma*, J. Biol. Phys., 48(4) (2022), 439–459.

[18] Hollon, T., Hervey-Jumper, S.L., Sagher, O. and Orringer, D.A. *Advances in the surgical management of low-grade glioma*, Semin. Radiat. Oncol., 25(3) (2015), 181–188.

[19] Jaber, T., and Balatif, O. *A mathematical model of drug-resistant cancer with cell cycle structure: stability, optimal control, and cost-effectiveness analysis*, Int. J. Dyn. Control, 13(10) (2025), 354.

[20] Jakola, A.S., Skjulsvik, A.J., Myrmel, K.S., Sjåvik, K., Unsgård, G., Torp, S.H., Aaberg, K., Berg, T., Dai, H.Y., Johnsen, K. and Kloster, R. *Surgical resection versus watchful waiting in low-grade gliomas*, Ann. Oncol., 28(8) (2017), 1942–1948.

[21] Khajanchi, S. *Stability analysis of a mathematical model for glioma-immune interaction under optimal therapy*, Int. J. Nonlin. Sci. Numer. Simul., 20(3-4) (2019), 269–285.

[22] Khalil, H.K. and Grizzle, J.W. *Nonlinear systems*, 3rd ed., Upper Saddle River, NJ: Prentice Hall, 2002.

[23] Kopp, R.E. *Pontryagin maximum principle*, in: Mathematics in Science and Engineering, Vol. 5, Amsterdam: Elsevier, (1962), 255–279.

[24] Kurzweil, J. *Ordinary differential equations: Introduction to the theory in the real domain*, Amsterdam: Elsevier, 2014.

[25] La Salle, J.P. *The Stability of dynamical systems*, Philadelphia: SIAM, 1976.

[26] Ledzewicz, U., and Schättler, H. *Analysis of a mathematical model for low-grade gliomas under chemotherapy as a dynamical system*, Nonlinear Anal. Real World Appl., 85 (2025), 104344.

[27] Louis, D.N., Perry, A., Wesseling, P., Brat, D.J., Cree, I.A., Figarella-Branger, D., Hawkins, C., Ng, H.K., Pfister, S.M., Reifenberger, G. and Soffietti, R. *The 2021 WHO classification of tumors of the central nervous system: a summary*, Neuro Oncol., 23(8) (2021), 1231–1251.

[28] McAsey, M., Mou, L. and Han, W. *Convergence of the forward-backward sweep method in optimal control*, Comput. Optim. Appl., 53(1) (2012), 207–226.

[29] McDuff, S.G., Dietrich, J., Atkins, K.M., Oh, K.S., Loeffler, J.S. and Shih, H.A. *Radiation and chemotherapy for high-risk lower grade gliomas: choosing between temozolomide and PCV*, Cancer Med., 9(1) (2020), 3–11.

[30] Mellinghoff, I.K., Van Den Bent, M.J., Blumenthal, D.T., Touat, M., Peters, K.B., Clarke, J., Mendez, J., Yust-Katz, S., Welsh, L., Mason, W.P. and Ducray, F. *Vorasidenib in IDH1- or IDH2-mutant low-grade glioma*, N. Engl. J. Med., 389(7) (2023), 589–601.

[31] Minniti, G., Paolini, S., Antonelli, M., Gianno, F., Tini, P., Lanzetta, G., Arcella, A., De Pietro, R., Giraffa, M., Capone, L. and Romano, A. *Long-term treatment outcomes of temozolomide-based chemoradiation in patients with adult-type diffuse IDH-mutant grade 2 astrocytoma*, J. Neurooncol., 164(2) (2023), 331–339.

[32] Nagumo, M. *Über die lage der integralkurven gewöhnlicher differentialgleichungen*, Proc. Phys Math. Soc. Jpn., 24 (1942), 551–559.

[33] Pace, A., Vidiri, A., Galie, E., Carosi, M., Telera, S., Cianciulli, A.M., Canalini, P., Giannarelli, D., Jandolo, B. and Carapella, C.M. *Temozolomide chemotherapy for progressive low-grade glioma: clinical benefits and radiological response*, Ann. Oncol., 14(12) (2003), 1722–1726.

[34] Patel, S.H., Bansal, A.G., Young, E.B., Batchala, P.P., Patrie, J.T., Lopes, M.B., Jain, R., Fadul, C.E. and Schiff, D. *Extent of surgical resection in lower-grade gliomas: differential impact based on molecular subtype*, AJNR Am. J. Neuroradiol., 40(7) (2019), 1149–1155.

[35] Reuvers, M.J., Burgers, V.W., Koekkoek, J.A., Brandsma, D., Compter, A., Kouwenhoven, M.C., van den Bent, M.J., Frissen, S.A., Husson, O. and van der Graaf, W.T. *Aiming at a moving target the daily life experiences of adolescents and young adults with a low-grade glioma*, Neurooncol. Pract., 12(1) (2025), 113–121.

[36] Ribba, B., Kaloshi, G., Peyre, M., Ricard, D., Calvez, V., Tod, M., Čajavec-Bernard, B., Idbaih, A., Psimaras, D., Dainese, L. and Pallud, J. *A tumor growth inhibition model for low-grade glioma treated with chemotherapy or radiotherapy*, Clin. Cancer Res., 18(18) (2012), 5071–5080.

[37] Shaw, E.G., Wang, M., Coons, S.W., Brachman, D.G., Buckner, J.C., Stelzer, K.J., Barger, G.R., Brown, P.D., Gilbert, M.R. and Mehta, M.P. *Randomized trial of radiation therapy plus procarbazine, lomustine, and vincristine chemotherapy for supratentorial adult low-grade glioma: initial results of RTOG 9802*, J. Clin. Oncol., 30(25) (2012), 3065–3070.

[38] Spitaels, J., Devriendt, D., Sadeghi, N., Luce, S., De Witte, O., Goldman, S., Mélot, C. and Lefranc, F. *Management of supratentorial recurrent low-grade glioma: a multidisciplinary experience in 35 adult patients*, Oncol. Lett., 14(3) (2017), 2789–2795.

[39] Teng, C., Zhu, Y., Li, Y., Dai, L., Pan, Z., Wanggou, S. and Li, X. *Recurrence- and malignant progression-associated biomarkers in low-grade gliomas and their roles in immunotherapy*, Front. Immunol., 13 (2022), 899710.

[40] Van den Driessche, P., and Watmough, J. *Reproduction numbers and sub-threshold endemic equilibria for compartmental models of disease transmission*, Math. Biosci., 180(1-2) (2002), 29–48.

[41] Wan, Q., Wu, X., Zhou, J., Wu, W., Cao, Y., Sun, C., Li, Z., Gong, Z., Tang, H., Li, Q. and Chu, J. *The hypoxia-associated high-risk cell subpopulation distinctly enhances the progression of glioma*, Adv. Sci., 12(17) (2025), 2416231.